Article

Cell Reports

Golgi Outpost Synthesis Impaired by Toxic Polyglutamine Proteins Contributes to Dendritic Pathology in Neurons

Graphical Abstract

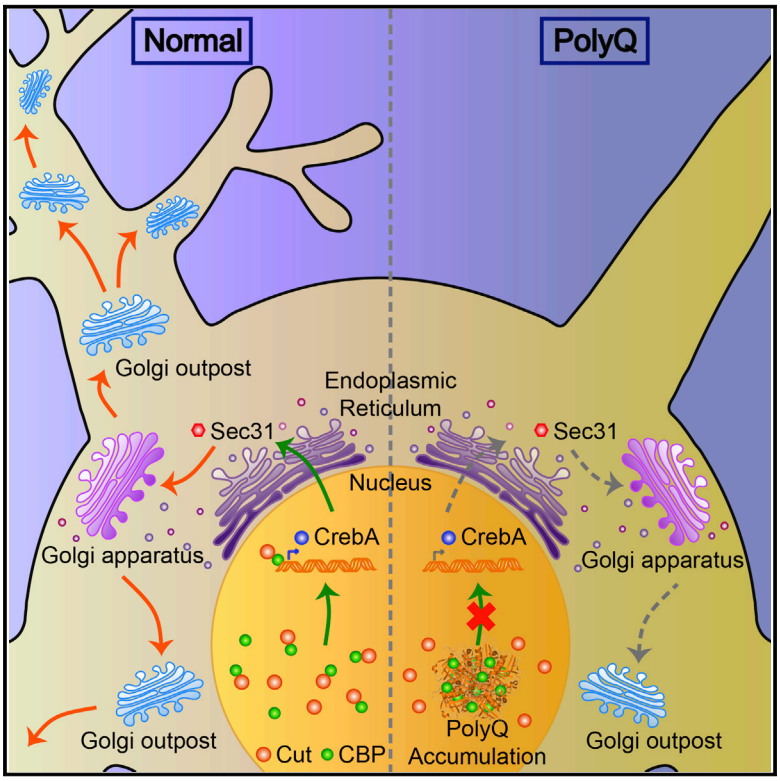

Highlights

- Nuclear polyQ toxicity induces dendritic pathology involving loss of Golgi outposts
- CrebA restores polyQ-induced dendritic pathology through COPII pathway
- CBP directly regulates *CrebA* transcription in cooperation with Cut
- PolyQ inhibits CBP at the upstream of CrebA in regulating Golgi outpost synthesis

Authors

Chang Geon Chung, Min Jee Kwon, Keun Hye Jeon, ..., Michael D. Ehlers, Daehee Hwang, Sung Bae Lee

Correspondence

dhwang@dgist.ac.kr (D.H.), sblee@dgist.ac.kr (S.B.L.)

In Brief

Chung et al. show that polyQ toxicity induces dendritic pathology involving loss of Golgi outposts (GOPs) in neurons. Genomic analysis reveals that polyQ inhibits expression of genes in the COPII pathway and GOP synthesis by blocking CBP and downregulating CREB3L1/CrebA expression. Enhancing CrebA restores COPII gene expression and GOP synthesis.

Accession Numbers

GSE65538

Chung et al., 2017, Cell Reports *20*, 356–369
July 11, 2017
http://dx.doi.org/10.1016/j.celrep.2017.06.059

CellPress

OPEN ACCESS
CellPress

Cell Reports
Article

Golgi Outpost Synthesis Impaired by Toxic Polyglutamine Proteins Contributes to Dendritic Pathology in Neurons

Chang Geon Chung,[1,9] Min Jee Kwon,[1,9] Keun Hye Jeon,[1,2,9] Do Young Hyeon,[3,9] Myeong Hoon Han,[1] Jeong Hyang Park,[1] In Jun Cha,[1] Jae Ho Cho,[1] Kunhyung Kim,[4] Sangchul Rho,[5] Gyu Ree Kim,[1] Hyobin Jeong,[5] Jae Won Lee,[6] TaeSoo Kim,[7] Keetae Kim,[4] Kwang Pyo Kim,[6] Michael D. Ehlers,[8] Daehee Hwang,[3,4,5,*] and Sung Bae Lee[1,10,*]

[1]Department of Brain and Cognitive Sciences, DGIST, Daegu 42988, Republic of Korea
[2]Department of Family Medicine, Samsung Medical Center, Seoul 06351, Republic of Korea
[3]School of Interdisciplinary Bioscience and Bioengineering, POSTECH, Pohang 37673, Republic of Korea
[4]Department of New Biology, DGIST, Daegu 42988, Republic of Korea
[5]Center for Plant Aging Research, Institute for Basic Science, DGIST, Daegu 42988, Republic of Korea
[6]Department of Applied Chemistry, Institute of Natural Science, College of Applied Science, Kyung Hee University, Yongin 17104, Republic of Korea
[7]Department of Life Science and the Research Center for Cellular Homeostasis, Ewha Womans University, Seoul 03760, Republic of Korea
[8]Biogen, 225 Binney Street, Cambridge, MA 02142, USA
[9]These authors contributed equally
[10]Lead Contact
*Correspondence: dhwang@dgist.ac.kr (D.H.), sblee@dgist.ac.kr (S.B.L.)
http://dx.doi.org/10.1016/j.celrep.2017.06.059

SUMMARY

Dendrite aberration is a common feature of neurodegenerative diseases caused by protein toxicity, but the underlying mechanisms remain largely elusive. Here, we show that nuclear polyglutamine (polyQ) toxicity resulted in defective terminal dendrite elongation accompanied by a loss of Golgi outposts (GOPs) and a decreased supply of plasma membrane (PM) in *Drosophila* class IV dendritic arborization (da) (C4 da) neurons. mRNA sequencing revealed that genes downregulated by polyQ proteins included many secretory pathway-related genes, including COPII genes regulating GOP synthesis. Transcription factor enrichment analysis identified *CREB3L1/CrebA*, which regulates COPII gene expression. CrebA overexpression in C4 da neurons restores the dysregulation of COPII genes, GOP synthesis, and PM supply. Chromatin immunoprecipitation (ChIP)-PCR revealed that *CrebA* expression is regulated by CREB-binding protein (CBP), which is sequestered by polyQ proteins. Furthermore, co-overexpression of CrebA and Rac1 synergistically restores the polyQ-induced dendrite pathology. Collectively, our results suggest that GOPs impaired by polyQ proteins contribute to dendrite pathology through the CBP-CrebA-COPII pathway.

INTRODUCTION

Neurons have tremendously higher amounts of plasma membrane (PM) than other cell types, due to their highly elongated morphology (Pfenninger, 2009). Recently, dendritic satellite organelles have been reported to be involved in the maintenance of integrity and dynamics of the PM in distal dendrites out of reach from somatic perinuclear organelles (Hanus and Ehlers, 2008; Pfenninger, 2009). The dendritic organelles have functional overlaps with the canonical perinuclear organelles (Hanus and Ehlers, 2008; Zhou et al., 2014). However, the restricted space appears to require the miniaturization of the satellite organelle systems, such as the endoplasmic reticulum (ER) and Golgi outposts (GOPs), compared to those localized around the nucleus, suggesting that the dendritic organelles may show different functional capacity from their perinuclear counterparts. Additionally, the distal areas of the dendrites may have quite different cellular environments, such as variations in the concentration of ions and proteins, compared to the perinuclear region. These differences may account for the vulnerability of dendrites over other neuronal domains to neuropathological insults, including protein toxicity conferred by the accumulation of mutant or misfolded proteins in neurons (Hasel et al., 2015; Kweon et al., 2017).

In *Drosophila* dendritic arborization (da) sensory neurons, GOPs were found to be located in dendrites, but not in axons, suggesting that GOPs may act as local stations to supply membranes to the PM in nearby dendrites (Ye et al., 2007). The synthesis of GOPs was reported to be regulated by secretory pathway-related genes, such as *Sec31* and the transcription factor *Cut* (Iyer et al., 2013). Additionally, GOPs were shown to be transported toward or away from the soma by machinery consisting of a lava lamp protein (LVA), a golgin coiled-coil adaptor protein, and a motor dynein-dynactin protein complex, and their transport was found to be closely associated with the dynamics of dendrite growth (Papoulas et al., 2005; Ye et al., 2007). Moreover, GOPs have been implicated in the growth and maintenance of the dendrite arbor. For example, laser ablation of local GOPs decreased branch dynamics in da neurons (Ye et al.,

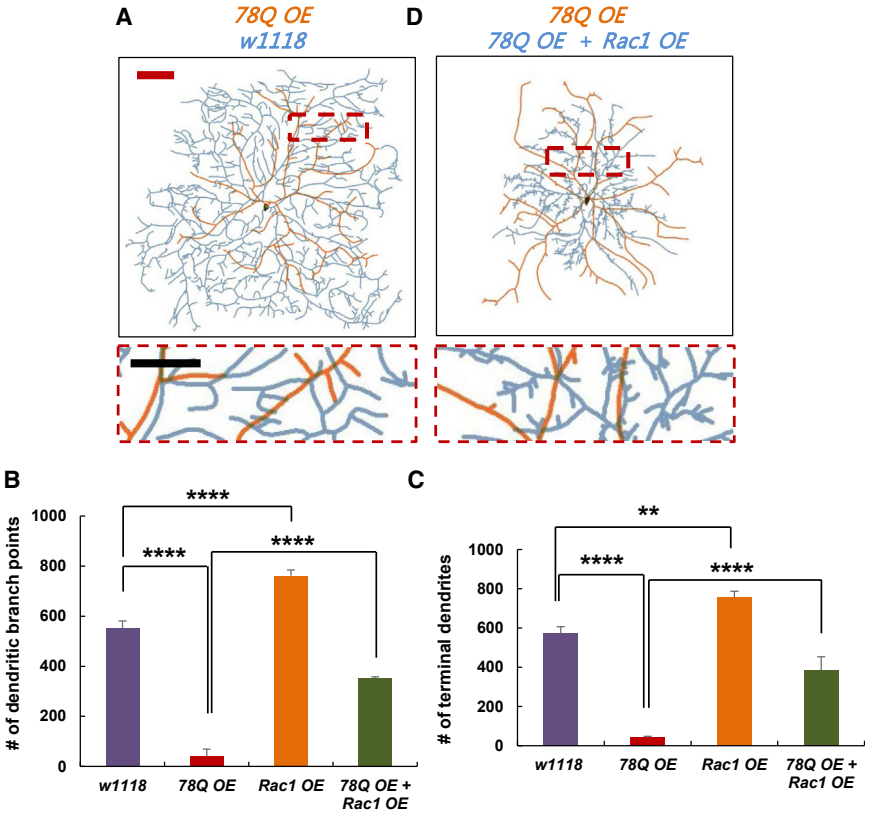

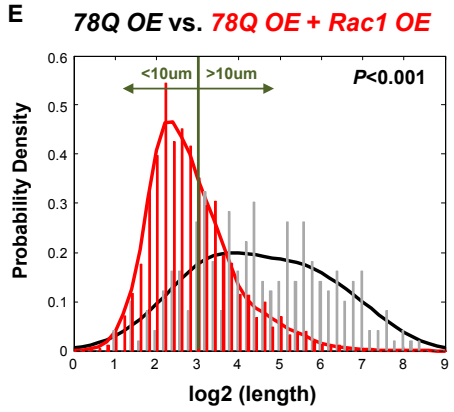

Figure 1. Rac1 Overexpression Preferentially Contributes to the Formation of Short Terminal Dendrites in PolyQ-Expressing C4 da Neurons

(A and D) Comparison of dendrite traces of representative C4 da neurons expressing the denoted transgenes: 78Q *OE* (orange) versus wild-type control *w1118* (light blue; A), 78Q *OE* (orange) versus *78Q OE* + *OE Rac1 OE* (light blue; D). Red insets are magnified in the bottom. The red scale bar represents 100 μm and black scale bar represents 50 μm.

(B and C) Comparisons of the number of dendritic branch points (B) and the number of terminal dendrites (C) in *w1118* and C4 da neurons expressing the denoted transgenes. $^{**}p < 0.01$; $^{****}p < 0.10 \times 10^{-3}$ by two-way ANOVA with Tukey's post hoc correction; error bars, SEM; n = 6.

(E) Comparison of the probability density functions (PDFs) of $\log_2$ (length of terminal dendrites) in C4 da neurons expressing the denoted transgenes: *78Q OE* (black) versus *78Q OE* + *Rac1 OE* (red). Normalized histograms are also provided. The p value represents the significance of the difference between the two PDFs from an empirical Kolmogorov-Smirnov (KS) test (Supplemental Experimental Procedures). Short (<10 μm) and longer (>10 μm) terminal dendrites are partitioned by a green line at 10 μm.

See also Figure S1.

Drosophila da sensory neurons that have been extensively utilized by various researchers as an in vivo cellular model for the study of the mammalian neuronal dendrite system with high fidelity (Jan and Jan, 2010).

RESULTS

Nuclear PolyQ Toxicity Disrupts Branching and Elongation of Terminal Dendrites

We first analyzed morphological characteristics of dendrites of class IV (C4) da neurons expressing pathogenic Machado-Joseph's Disease (MJD) protein, MJDtr-78Q (78Q), known to induce nuclear protein toxicity. For this analysis, we compared dendrite images of C4 da neurons expressing 78Q (*78Q OE*; n = 6) and wild-type C4 da neuron controls (*w1118*; n = 6; Figures 1A and S1A–S1G). The comparison showed a significant ($p < 0.10 \times 10^{-3}$) reduction in the number of dendritic branch points (Figure 1B) in *78Q OE* compared to *w1118*. Consistently, the number of terminal dendrites, another feature of dendritic branching, significantly ($p < 0.10 \times 10^{-3}$) decreased in *78Q OE* (average = 41.33) compared to *w1118* (average = 573.00; Figure 1C). On the other hand, previously, time-lapse imaging of terminal dendrites in C4 da neurons revealed that the growth (elongation) of terminal dendrites was decreased in *78Q OE* compared to *w1118* (Lee et al., 2011).

2007), and the disruption of GOP trafficking blocked dendrite growth in developing hippocampal neurons, leading to the decreased length of dendrites (Horton et al., 2005).

Despite such functional roles of the GOPs in the growth and maintenance of the dendrite arbor under non-pathological conditions, it still remains unclear whether the GOPs can also contribute to dendrite aberration observed under pathological conditions induced by protein toxicity. Previously, nuclear proteotoxicity has been reported to cause severe dendrite pathology (Lee et al., 2011), but the mechanisms underlying dendrite pathology caused by protein toxicity remain largely elusive. We therefore investigated a mechanistic link of the GOPs to dendrite pathology caused by toxic nuclear polyQ proteins using

Taken together, these data collectively suggest that polyQ proteins inhibit both the branching and elongation of terminal dendrites.

The decreased number of dendritic branch points by polyQ proteins was previously shown to be restored in C4 da neurons via the co-overexpression of 78Q and Rac1, an upstream regulator of F-actin polymerization (*78Q OE* + *Rac1 OE*; Lee et al., 2011). Consistent with this previous observation, we found that *78Q OE* + *Rac1 OE* showed a significant increase in the number of dendritic branch points (Figure 1B) and of terminal dendrites (Figures 1C and 1D) compared to *78Q OE*, and Rac1 overexpression alone in C4 da neurons (*Rac1 OE*) also showed an increase in dendritic branch points compared to *w1118* (Figures 1B and 1C). However, it is not clear whether Rac1 can also contribute to the elongation of terminal dendrites in *78Q OE*, in addition to the effects on branching. To examine this aspect, we further compared the length distributions of individual terminal dendrites between *78Q OE* and *78Q OE* + *Rac1 OE* (Figures S1H and S1I). Interestingly, probability density functions (PDFs) of terminal dendritic lengths showed a significantly ($p < 1.0 \times 10^{-3}$) higher proportion of short terminal dendrites (<10 μm) in *78Q OE* + *Rac1 OE* compared to *78Q OE* (Figure 1E). This pattern was also observed in *Rac1 OE* compared to *w1118* (Figures S1J–S1L). These data suggest that Rac1 can contribute more predominantly to the formation of short terminal dendrites (branching) than the formation of long terminal dendrites (elongation) in *78Q OE*.

Nuclear PolyQ Toxicity Induces a Loss of GOPs

Next, we questioned what additional factors are required for the formation of long terminal dendrites in *78Q OE*. It was previously shown that laser ablation of GOPs reduced the growth of terminal dendrites in C4 da neurons, suggesting a potential link between GOPs and dendrite elongation (Ye et al., 2007). Based on this observation, we then examined whether the disruption of GOPs occurred in polyQ-expressing neurons together with the impairment in terminal dendrite elongation induced by toxic polyQ proteins. To this end, we first compared the localization of ManII-eGFP puncta, which marks the medial Golgi compartment, between *78Q OE*, *27Q OE* (C4 da neurons expressing non-expanded MJD protein), and *w1118*. *78Q OE* (n = 12) showed a significantly decreased number of GOPs in both primary and secondary dendrites compared to *w1118* (n = 12) and *27Q OE* (Figures 2A and 2B). By contrast, the number of GOPs was not significantly different in *27Q OE* and *w1118*. Henceforth, we used *w1118* as the control for *78Q OE*.

Furthermore, we examined whether the loss of GOPs is specifically caused by 78Q by measuring the number of GOPs in C4 da neurons expressing two other polyQ constructs that induce nuclear protein toxicity, MJDFL-78Q (pathogenic MJD full-length protein) and Ataxin1-82Q (pathogenic spinocerebellar ataxia type 1 protein). A comparison of the number of GOPs showed similar decreases in the number of GOPs in C4 da neurons expressing these constructs (Figures S2A and S2B), suggesting that the loss of GOPs is not caused only by 78Q but also by other toxic nuclear polyQ proteins. Interestingly, polyQ proteins caused no noticeable structural alterations in the somatic Golgi in C4 da neurons (Figure 2A) or in the dorsal da neuronal clusters (Figure 2C), suggesting a preferential malformation of dendritic GOPs over somatic Golgi. Finally, we examined whether the polyQ-induced pathology of dendrites and GOPs was also observed in mammalian hippocampal primary neurons. To this end, rat hippocampal primary neurons were transfected with pGolt-mCherry, which labels GOPs and Golgi satellites (GSs) (Mikhaylova et al., 2016). We observed that pGolt-mCherry-positive dendritic Golgi (GOPs and/or GSs) in rat hippocampal primary neurons showed widespread distributions that are comparable to those of ManII-eGFP-positive GOPs in C4 da neurons (Figure S2E). Consistent with the *Drosophila* data, in rodent hippocampal primary neurons, transfection of MJD-75Q significantly reduced the number of dendritic spines (Figures S2C and S2D) and pGolt-mCherry-positive dendritic Golgi puncta (Figure S2E) compared to the controls.

Dendritic GOPs have been shown to supply proteins and lipids to the PM, thereby contributing to dendrite growth and maintenance (Horton et al., 2005; Ye et al., 2007). Thus, we examined whether the PM protein supply was also affected by toxic polyQ proteins by comparing the normalized fluorescence intensities of a membrane marker protein, mCD8-GFP (Murthy et al., 2005), by those of nucleus-targeted Redstinger (mCherry-NLS) between *78Q OE* and *w1118*. The normalized intensity of mCD8-GFP, similar to the number of GOPs (Figure 2B), markedly (~60%) decreased in *78Q OE* compared to *w1118* (Figures 2D and 2E). On the other hand, CD4-tdGFP has recently been shown to serve as an alternative membrane marker with stronger and more even expression throughout dendrites compared to mCD8-GFP (Han et al., 2011). The intensity of CD4-tdGFP showed a consistent decrease in *78Q OE* compared to *w1118* (Figure S2F). Moreover, we also examined whether the decreased PM protein supply was specifically caused by 78Q by measuring the PM protein supply in C4 da neurons expressing MJDFL-78Q and Ataxin1-82Q. Similar decreases in the intensity of CD4-tdGFP were observed in these neurons compared to the controls (Figure S2F). Taken together, these data suggest that nuclear polyQ toxicity results in the decrease in GOP synthesis and PM protein supply.

Nuclear PolyQ Toxicity Downregulates Cellular Processes Associated with GOP Synthesis and PM Protein Supply

To investigate the processes that are associated with the polyQ-induced loss of GOPs, we next performed mRNA sequencing of fly heads with or without 78Q expression (Figure 3A). From the mRNA sequencing data, we identified 5,385 differentially expressed genes (DEGs) ($p < 0.05$) between the polyQ-expressed and control samples (Table S1) using a previously described statistical method (Chae et al., 2013). Of the 5,385 DEGs, 98.9% (5,325 genes) were downregulated in the polyQ-expressed condition (see Discussion), suggesting that nuclear polyQ toxicity decreased the activities of cellular processes associated with DEGs.

To understand the cellular processes disrupted by toxic polyQ proteins, we performed an enrichment analysis of gene ontology biological processes (GOBPs) for the 5,325 downregulated genes using DAVID software (Huang da et al., 2009; Table S2). The downregulated genes were involved in a broad spectrum of cellular processes (Figure 3B). Of them, we focused on the following processes potentially associated with GOPs: (1) vesicle-mediated

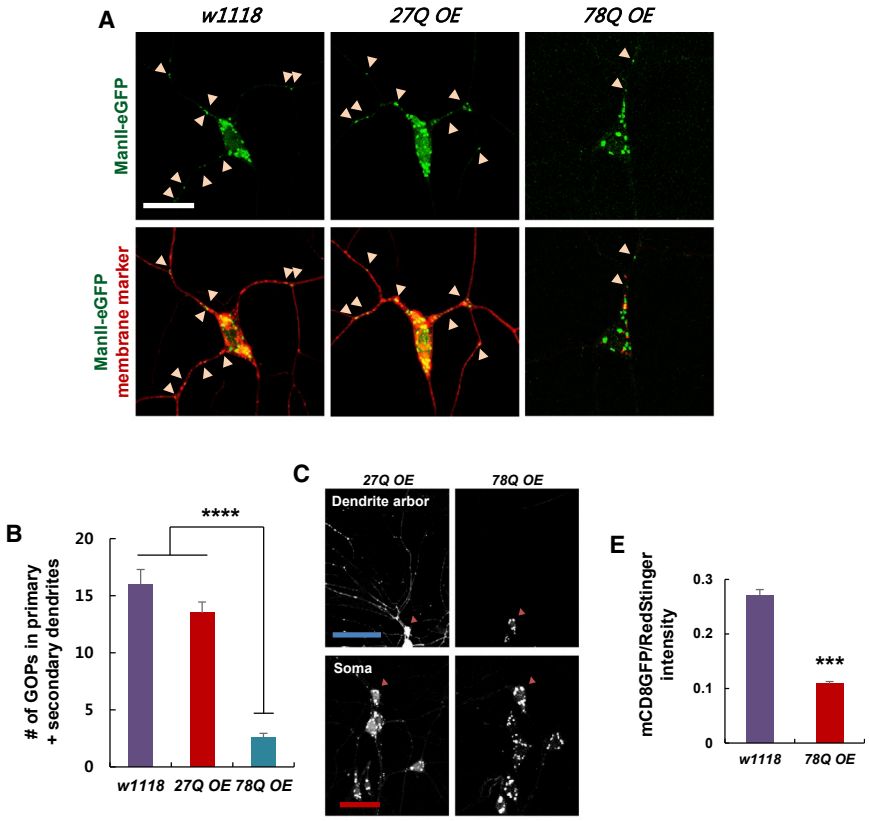

Figure 2. PolyQ Toxicity Results in a Loss of GOPs

(A) Representative images of GOPs in *w1118* and C4 da neurons expressing *27Q* (*27Q OE*) and *78Q* (*78Q OE*). The medial Golgi marker (ManII-eGFP) and plasma membrane (PM) marker (CD4-tdTom) were expressed to visualize GOPs and dendrites, respectively. GOPs are indicated by arrowheads. The scale bar represents 20 μm.

(B) Quantification of the number of GOPs in both primary and secondary dendrites of *w1118*, *27Q OE*, and *78Q OE*. ****$p < 0.10 \times 10^{-3}$ by one-way ANOVA with Tukey's post hoc correction; error bars, SEM; n = 12.

(C) Representative black and white images of GOPs labeled by ManII-eGFP in dorsal da neuronal clusters expressing the denoted transgenes. Somatic Golgi are indicated by arrowheads. The blue scale bar represents 50 μm and red scale bar represents 20 μm.

(D) Images of Redstinger (mCherry-NLS) and mCD8-GFP in *78Q OE* and *w1118*. Due to weak fluorescence intensity, images converted to HiLo via ImageJ for *78Q OE* are also shown. Soma are outlined by white dotted lines. The scale bar represents 25 μm.

(E) Quantification of mCD8-GFP fluorescence intensity normalized to that of Redstinger's in *w1118* and *78Q OE*. ***$p < 0.001$ by Student's t test; error bars, SEM; $n \geq 10$.

See also Figure S2.

transport (VT) and (2) membrane organization (MO). Notably, they were among the most significantly affected cellular processes (Figure 3B). Moreover, among the daughter GOBPs of VT, ER-to-Golgi transport was strongly affected by polyQ toxicity (Figures 3C and 3D), consistent with the loss of GOPs caused by polyQ expression (Figures 2A and 2B). Additionally, among the daughter GOBPs of MO, PM organization was strongly affected by polyQ toxicity (Figures 3E and 3F), consistent with decreased PM protein targeting by polyQ expression (Figures 2D and 2E). Next, we confirmed the downregulation of the following six representative genes by polyQ protein expression using RT-PCR analysis of independent sets of fly heads ($n \geq 3$; Figure 3G): *Sec13*; *Sec23*; *Sec31*; *Sec63*; and *CrebA* involved in VT and *Rac1* involved in MO.

Lipid metabolism is intricately involved in the synthesis and function of Golgi apparatus (Bankaitis et al., 2012). Thus, we reasoned that the disruption of lipid metabolism could likely impinge on Golgi apparatus. Indeed, many genes involved in the lipid biosynthetic process (LP) and its daughter GOBPs were downregulated by toxic polyQ proteins (Figures 3B, S3A, and S3B). Based on this observation, we next examined whether toxic polyQ proteins caused alterations in the levels of PM lipids. Using the mass-spectrometry-based method previously described (Hong et al., 2016), we compared the levels of two lipids present in PM, sphingomyelin (SM) and phosphatidylcholine (PC) (van Meer et al., 2008) with and without polyQ expression in adult fly whole-brain extracts. The level of SM, which is associated with the PM supply through the secretory pathway (Koval and Pagano, 1991), was significantly decreased by 78Q (Figures S3C and S3D). The level of PC was also decreased, similar to SM (Figures S3E and S3F). The decreases in SM and PC were further confirmed with an independent lipid assay kit (Figure S3G). Taken together, these data suggest that nuclear polyQ toxicity significantly disrupts cellular processes associated with GOP synthesis and PM protein supply.

CrebA Overexpression Restores the Downregulation of COPII Pathway and the Loss of GOPs Caused by Nuclear PolyQ Toxicity

A growing volume of evidence suggests that the genes involved in the secretory pathway contribute to the synthesis and

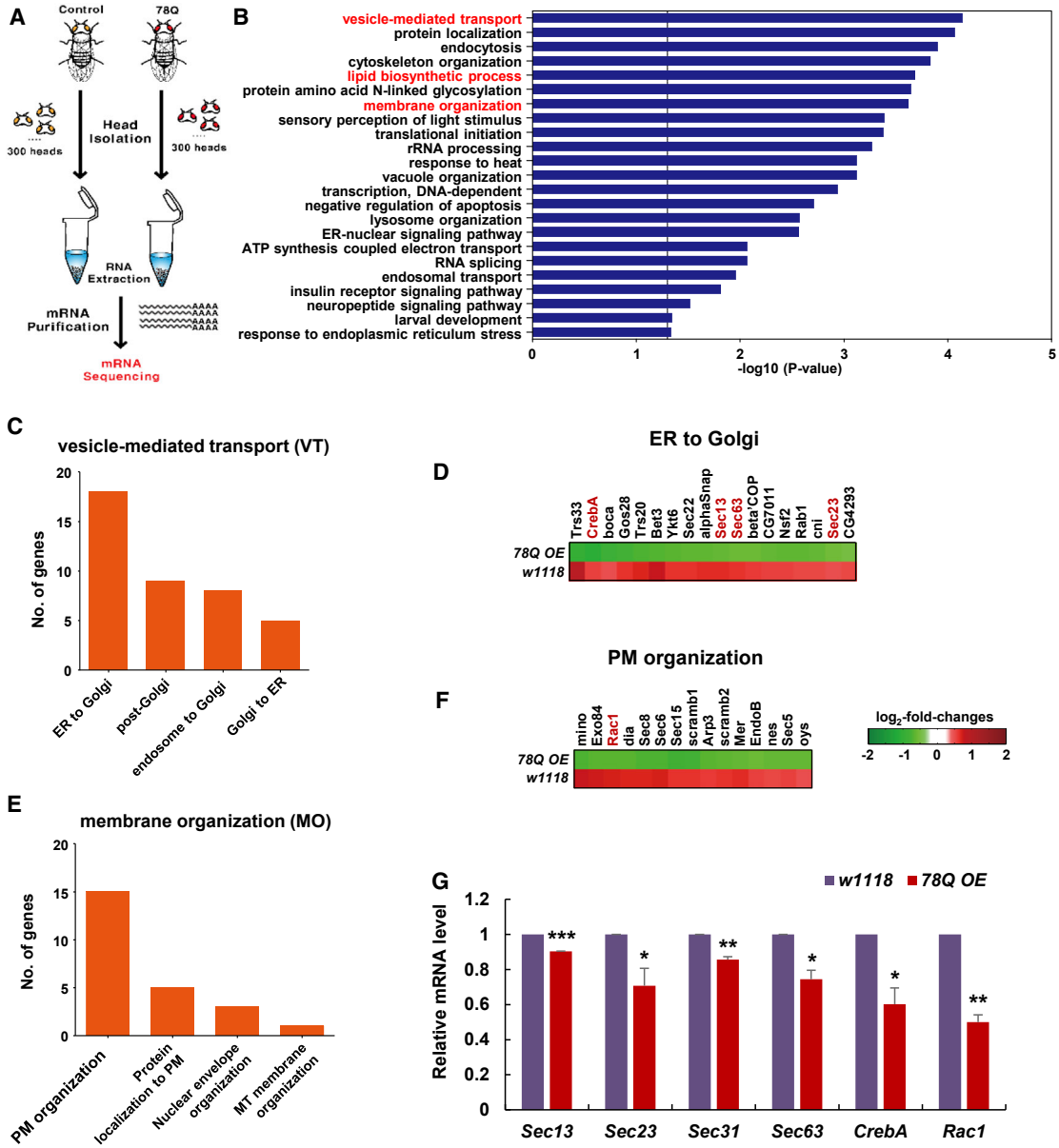

Figure 3. PolyQ Toxicity Downregulates Cellular Processes Associated with GOP Synthesis and PM Protein Supply

(A) Experimental scheme for mRNA sequencing of *78Q OE* and *w1118* (control) fly heads.

(B) GOBPs represented by the downregulated genes in *78Q OE*, compared to *w1118*. The p value is the significance of the GOBPs being enriched by the downregulated genes from DAVID software. Three GOBPs associated with GOP synthesis are highlighted in red.

(C–F) The number (C and E) of downregulated genes involved in daughter GOBPs of vesicle-mediated transport (VT) (C) and membrane organization (MO) (E). (D and F) Heatmap representations of downregulated genes involved in ER to Golgi (D) and PM organization (F) and daughter GOBPs of VT and MO, respectively. The color bar in the heatmap represents gradient of $\log_2$-fold changes of mRNA expression levels in *78Q OE* and *w1118* with respect to the median mRNA expression levels.

(G) Relative mRNA expression levels of the denoted genes in *78Q OE* with respect to those in *w1118*. *$p < 0.05$; **$p < 0.01$; ***$p < 0.001$ by Student's t test; error bars, SEM; $n \geq 3$.

See also Figure S3 and Tables S1 and S2.

maintenance of GOPs (Hanus and Ehlers, 2008; Iyer et al., 2013; Ye et al., 2007). Moreover, our mRNA-sequencing data also showed that polyQ proteins led to the downregulation of genes involved in the secretory pathway (*Sec13*, *Sec23*, *Sec31*, and *Sec63*). These data suggest that the transcriptional dysregulation of the secretory pathway may be linked to the loss of GOPs caused by nuclear polyQ toxicity in C4 da neurons. To test this hypothesis, we examined the number of GOPs and

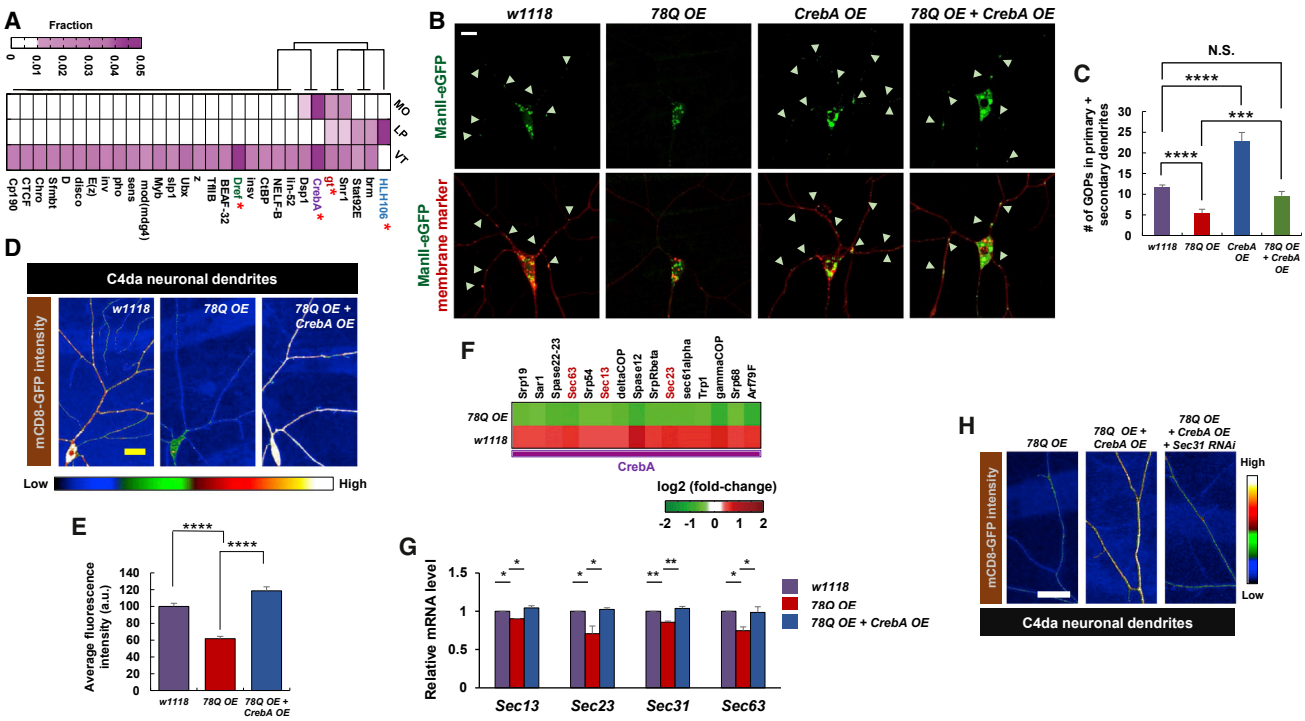

Figure 4. CrebA Overexpression Restores the Downregulation of the COPII Pathway and the Loss of GOPs by Nuclear PolyQ Toxicity

(A) Twenty-nine TF candidates and the distribution of their targets in three GOBPs: MO; lipid biosynthetic process (LP); and VT. The color bar represents gradient of the number of downregulated targets in each GOBP divided by the total number of targets (target fraction). TFs were clustered using target fractions in the three GOBPs by hierarchical clustering (average linkage and Euclidean distance as a dissimilarity measure).

(B) Representative images of GOPs labeled by ManII-eGFP in *w1118* and C4 da neurons expressing the denoted transgenes. GOPs are indicated by arrowheads. The scale bar represents 10 μm.

(C) Quantification of the number of GOPs in both primary and secondary dendrites of *w1118* and C4 da neurons expressing the denoted transgenes. N.S., not significant; ***$p < 0.001$; ****$p < 0.10 \times 10^{-3}$ by two-way ANOVA with Tukey's post hoc correction; error bars, SEM; $n \geq 14$.

(D) Representative mCD8-GFP-labeled dendrite images (pseudocolored ThaI) in *w1118* and C4 da neurons expressing the denoted transgenes. The scale bar represents 20 μm.

(E) Quantification of mCD8-GFP pixel intensity in *w1118* and C4 da neurons expressing the denoted transgenes. ****$p < 0.10 \times 10^{-3}$ by one-way ANOVA with Tukey's post hoc correction; error bars, SEM; n = 8. Controls are normalized to 100.

(F) Downregulated targets of CrebA in *78Q OE*, compared to *w1118*. The color bar represents gradient of $\log_2$-fold changes of mRNA expression levels in *78Q OE* and *w1118* with respect to the median mRNA expression levels.

(G) Relative mRNA levels of *Sec13*, *Sec23*, *Sec31*, and *Sec63* in fly brains of *78Q OE*, *78Q OE + CrebA OE*, and *w1118*. *$p < 0.05$; **$p < 0.01$ by one-way ANOVA with Tukey's post hoc correction; error bars, SEM; n = 3.

(H) mCD8-GFP-labeled C4 da neuronal dendrites expressing the denoted transgenes (pseudocolored ThaI). The scale bar represents 50 μm.

See Figures S4 and S5 and Table S3.

the PM protein supply after the knockdown of *Sec23* and *Sec31*, key components of the COPII pathway (Paccaud et al., 1996; Salama et al., 1997). Knockdown of these genes significantly decreased the number of GOPs (Figures S4A and S4B). Moreover, knockdown of *Sec31* decreased the PM protein supply (Figures S4C and S4D). These results support our hypothesis that the disrupted COPII pathway can contribute to the loss of GOPs in polyQ-expressing neurons.

Next, we questioned what transcription factors (TFs) regulate the expression of genes involved in the secretory pathway or in GOP synthesis and the PM protein supply. To answer this question, we searched for key TFs regulating the genes involved in the aforementioned cellular processes compromised by nuclear polyQ toxicity: MO; VT; and LP. This search identified 29 TFs that were downregulated by nuclear polyQ toxicity, and a significant ($p < 0.05$) number of target genes were involved in the three processes (Figure 4A). Of the 29 candidate TFs, CrebA (CREB3L1; human ortholog; Fox et al., 2010) was found to regulate the largest fraction of the genes involved in MO and VT (Figure 4A) associated with PM protein supply (Figure 3E) and the COPII pathway (Figure 3C), respectively. Additionally, HLH106 (SREBP1; human ortholog; Theopold et al., 1996) was found to regulate the largest fraction of the genes involved in LP (Figure 4A). CrebA and HLH106 have been shown to act as the master regulators of the secretory pathways, including the COPII pathway (Table S3; Abrams and Andrew, 2005; Fox et al., 2010), and of lipid biosynthesis (Eberlé et al., 2004), respectively. Dref (DREF; human ortholog), a key regulator of cell proliferation (Matsukage et al., 2008), was also identified to regulate a significant fraction of the genes involved in VT, whereas gt, a regulator

of segmentation gap genes (Capovilla et al., 1992), was found to regulate a large fraction of the genes involved in all three processes (Figure 4A). We next examined whether their overexpression could restore the loss of GOPs and reduce the PM protein supply in *78Q OE*. C4 da neurons co-expressing 78Q and CrebA (*78Q OE* + *CrebA OE*) showed significant increases in the number of GOPs (Figures 4B and 4C) and in the PM protein supply (Figures 4D and 4E) compared to *78Q OE*. In contrast, overexpression of the other three TFs failed to restore the loss of GOPs (Figure S5A). Consistently, the overexpression of CrebA alone in C4 da neurons (*CrebA OE*) also significantly increased the number of GOPs (Figures 4B and 4C) compared to *w1118*.

Of the known target genes of CrebA (Table S3), 15 COPII pathway-related molecules (44.1% of 34 target genes) were downregulated by nuclear polyQ toxicity (Figure 4F). The downregulation of *CREB3L1*, a human ortholog of CrebA, and its two key downstream targets, *Sec13* and *Sec23*α (Fox et al., 2010), was further confirmed in HEK293T cells expressing MJD-77Q (Figure S5B). Thus, we next examined whether CrebA overexpression could restore the downregulation of the four representative COPII pathway-related CrebA target genes (*Sec13*, *Sec23*, *Sec31*, and *Sec63*) caused by nuclear polyQ toxicity using RT-PCR analysis. The expression levels of these genes were restored to levels comparable to those in the *w1118* fly heads (Figure 4G). Moreover, the restoration of the PM protein supply by CrebA overexpression was suppressed by the additional knockdown of *Sec31* (Figure 4H). Note that *Sec31*, a well-known COPII pathway gene, was included in these experiments, although it was not identified as a DEG from mRNA sequencing data due to its marginal significance ($p = 0.08$) of being downregulated. Taken together, these data suggest that CrebA overexpression restores the downregulation of the COPII pathway and the loss of GOPs caused by nuclear polyQ toxicity.

Co-overexpression of CrebA and Rac1 Synergistically Restores PolyQ-Induced Dendrite Pathology

We showed above that toxic polyQ proteins caused defects in the branching and elongation of terminal dendrites (Figure 1). Thus, we examined whether CrebA overexpression could restore such defects of terminal dendrites in polyQ-expressing neurons. To this end, we compared the number of terminal dendrites between *78Q OE* + *CrebA OE* and *78Q OE*. Interestingly, however, we found no significant difference in the number of terminal dendrites (branching) between *78Q OE* + *CrebA OE* and *78Q OE* (Figures 5A and S6A). To examine changes in the elongation of terminal dendrites, we then compared the distribution of terminal dendritic lengths between *78Q OE* + *CrebA OE* and *78Q OE* (Figure 5B) and found no significant ($p = 0.12$) difference in the distribution. These data collectively imply that no significant changes exist in the branching and elongation of terminal dendrites by CrebA overexpression.

We next questioned whether the restoration of polyQ-induced dendritic defects by CrebA required the preceding rescue of terminal dendrite branching in a CrebA-independent manner. We showed above that the overexpression of Rac1 restored terminal dendrite branching (Figure 1). Thus, we examined whether the co-overexpression of CrebA and Rac1 could restore the polyQ-induced defects in terminal dendrites. Indeed, a significant (53.85%) fraction of C4 da neurons co-overexpressing CrebA and Rac1 showed an increased formation of long (>10 μm) terminal dendrites compared to *78Q OE* (Figure 5C). On the other hand, only a marginal fraction (12.50%) of *78Q OE* overexpressing Rac1 alone showed the formation of long terminal dendrites compared to *78Q OE*, whereas a higher fraction (75.00%) showed the formation of short terminal dendrites (Figure 5C). Dendrites of C4 da neurons from each genotype that belong to the major fraction were chosen for subsequent comparisons. The comparison of the distribution of terminal dendritic lengths showed that *78Q OE* + *Rac1 OE* + *CrebA OE* (Figure S6B), compared to *78Q OE* + *Rac1 OE* (Figure S1I), showed a significant ($p < 0.01$) increase ($\sim$77.85%) in the formation of long terminal dendrites (Figures 5D, 5E, and S6C). Taken together, these data suggest that the co-overexpression of CrebA and Rac1 synergistically restores polyQ-induced dendrite pathology.

Previous studies showed that da sensory neurons play an important role in larval locomotion (Hughes and Thomas, 2007; Song et al., 2007), suggesting that 78Q-induced dendrite defects in da neurons might impair the functions of da neurons, such as larval locomotion. Thus, we examined the effect of the co-overexpression of Rac1 and CrebA on larval locomotion under the polyQ-expressed condition. We compared the locomotion of larvae with the overexpression of the following transgenes in the entire da neuronal cluster using 109(2)80-gal4 and the locomotion of control larvae (*w1118*; $n = 20$) by measuring the fractions of larvae that reached the edge of the petri dish within one min: *78Q*; *CrebA*; *78Q* + *CrebA*; *CrebA* + *Rac1*; and *78Q* + *Rac1* + *CrebA*. The fraction was significantly ($p = 0.01$) increased in *78Q* compared to *w1118*. According to our observations during the experiments, there appears to be no noticeable increase in speed but rather a decrease in the number of turns in *78Q* compared to *w1118*, indicating that 78Q expression likely impaired the ability of larva to turn. This alteration was restored by the co-overexpression of CrebA and Rac1 in *78Q* (Figure 5F), suggesting the contribution of Rac1 and CrebA to improving larval locomotion under the polyQ-expressed condition.

CBP Directly Binds to the *CrebA* Promoter to Regulate Its Transcription in Cooperation with Cut

We next questioned what TFs regulate the expression of *CrebA* and thus could account for the downregulation of *CrebA* in the polyQ-expressed condition. Previously, Cut (Iyer et al., 2013) and Scr (Henderson and Andrew, 2000) were reported as the upstream TFs of CrebA and another TF CREB-binding protein (CBP) was described as a genetic interactor of CrebA in the fly retinal system (CrebA mutant suppressed retinal degeneration induced by the overexpression of mutant CBP; Anderson et al., 2005). Thus, we tested whether the overexpression of Cut, Scr, and CBP could also restore the loss of GOPs, similar to CrebA overexpression, in polyQ-expressing neurons. We found that the overexpression of only CBP, among the three TFs, appeared to restore the loss of GOPs in polyQ-expressing neurons (Figure S7A). To further confirm this observation, we compared the number of GOPs in the following C4 da neurons: *w1118*; *CBP OE*; *78Q OE*; and *78Q OE* + *CBP OE*. Consistent with the above finding, CBP overexpression significantly

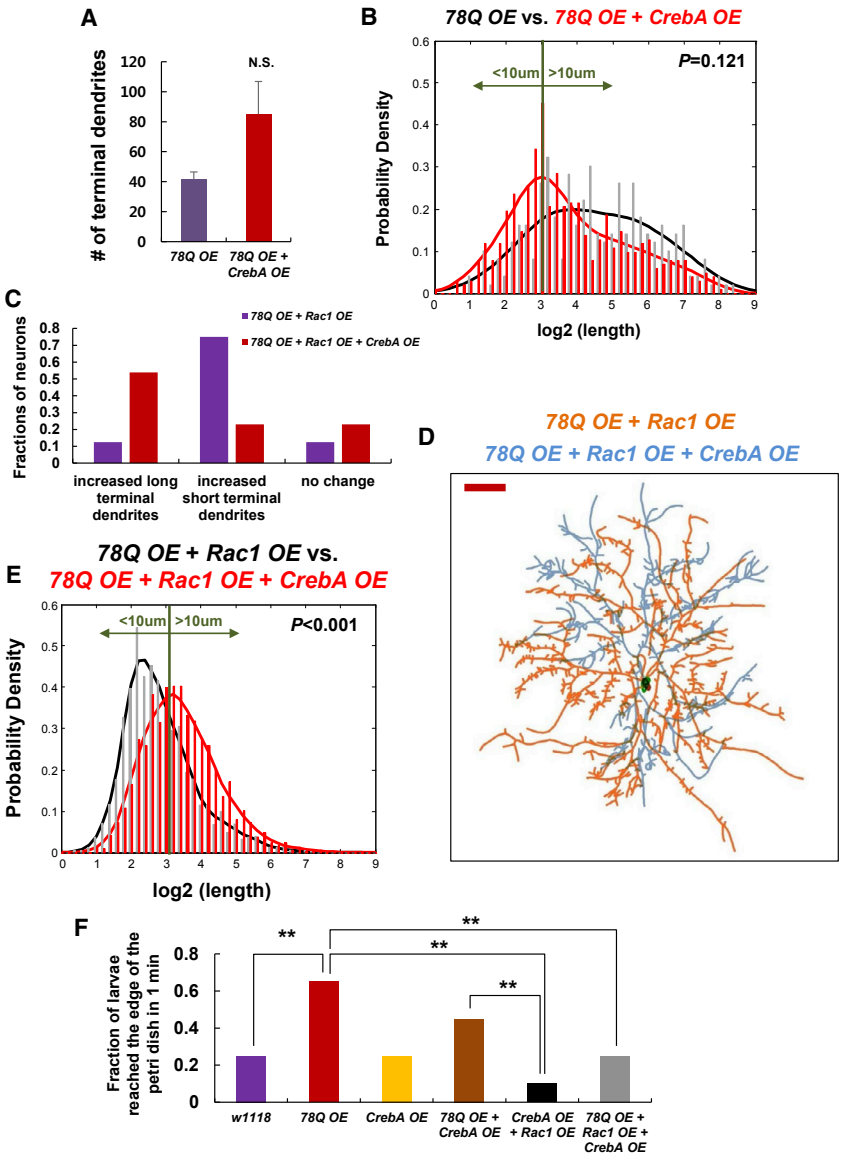

Figure 5. Co-overexpression of CrebA with Rac1 Synergistically Restores PolyQ-Induced Dendrite Defects

(A) Quantification of the number of terminal dendrites in *78Q OE* and *78Q OE + CrebA OE*. N.S., not significant by Student's t test; error bars, SEM; n = 6.

(B) Comparison of PDFs of $\log_2$ (length of terminal dendrites) in C4 da neurons expressing the denoted transgenes: *78Q OE* (black) versus *78Q OE + CrebA OE* (red). Normalized histograms were also provided with p values from the KS test. Short (<10 μm) and longer (>10 μm) terminal dendrites are partitioned by a green line.

(C) Fractions of C4 da neurons expressing the denoted transgenes, *78Q OE + Rac1 OE* (blue), and *78Q OE + Rac1 OE + CrebA OE* (red), which show increased short terminal dendrites, increased long terminal dendrites, or no change in terminal dendrites compared to *78Q OE*. n ≥ 8.

(D) Comparison of dendrite traces of representative C4 da neurons expressing the denoted transgenes: *78Q OE + Rac1 OE* (orange) versus *78Q OE + Rac1 OE + CrebA OE* (light blue). The scale bar represents 100 μm.

(E) Comparison of PDFs of $\log_2$ (length of terminal dendrites) in C4 da neurons expressing the denoted transgenes: *78Q OE + Rac1 OE* (black) versus *78Q OE + Rac1 OE + CrebA OE* (red). See the legend in (B).

(F) The percentage of larvae expressing the denoted transgenes (x axis) that reached the outer edge of the 90-mm petri dish within 1 min of starting from the center. n = 20. Random permutation experiments were performed to evaluate the statistical significance of the fraction difference between two genotypes (Supplemental Experimental Procedures).

See also Figure S6.

($p < 0.10 \times 10^{-3}$) restored the loss of GOPs in *78Q OE* (Figure 6A). In support of this finding, the knockdown and overexpression of CBP in C4 da neurons resulted in a significant decrease ($p < 0.10 \times 10^{-3}$) and increase ($p < 0.10 \times 10^{-3}$), respectively, in the number of GOPs compared to *w1118* (Figures 6B and 6C).

Next, we examined whether CBP directly binds to the promoter region of *CrebA* in CBP-overexpressed fly heads via chromatin immunoprecipitation (ChIP)-PCR analysis with four different sets of primers covering the promoter and 5′ UTR of *CrebA* (P1–P4 in Figure 6D). The binding strengths in CBP-overexpressed samples were significantly larger compared to *w1118* samples near the transcription start site (P3 and P4 in Figure 6D), suggesting the direct binding of CBP to the promoter region of *CrebA* (Figure 6D). To further confirm the regulation of *CrebA* by CBP, we measured the expression level of *CrebA* after the knockdown and overexpression of CBP in *w1118* fly heads. Consistent with the above data, CBP knockdown significantly ($p < 0.10 \times 10^{-3}$) decreased *CrebA* expression (Figure 6E). Interestingly, however, CBP overexpression did not significantly ($p = 0.9844$) change *CrebA* expression (Figure 6E), suggesting that CBP is necessary, but not sufficient, for *CrebA* transcription. Hence, we hypothesized that CBP required a co-factor to regulate *CrebA* transcription. Previously, CBP was shown via co-immunoprecipitation (coIP) to interact with Cut in HeLa cells (Li et al., 2000). Based on this observation, we checked whether CBP interacts with Cut in fly heads through coIP experiment and confirmed the interaction of CBP with Cut (Figure 6F). We then tested whether the knockdown of *Cut* could decrease the level of *CrebA* mRNA in fly brains and found that *Cut* knockdown significantly ($p < 0.01$) decreased the level of *CrebA* mRNA compared to controls (Figure 6G). Consistently, after the knockdown of *Cut*, significantly ($p < 0.05$) fewer GOPs were detected in C4 da neurons compared to controls (Figure 6H). We next examined whether the co-overexpression of CBP and Cut could increase the mRNA level of *CrebA* in fly heads. Indeed, *CrebA* expression was found to be significantly ($p < 0.001$) increased compared to fly heads overexpressing either CBP or Cut (Figure 6I). These

data altogether suggest that Cut and CBP act together to regulate *CrebA* transcription in the fly neuronal system, thereby contributing to GOP synthesis.

Nuclear PolyQ Proteins Interfere with CBP Upstream of CrebA in the Regulation of GOP Synthesis

Finally, we asked how CBP and/or Cut, the upstream regulators of *CrebA*, could be affected by 78Q. Toxic polyQ proteins are known to sequester interacting molecules, which possibly inhibits their functions (Orr and Zoghbi, 2007). CBP is a well-known polyQ interactor, and the histone acetylation activity of CBP was shown to be decreased under polyQ-expressed conditions (Hughes, 2002). Based on these observations, we hypothesized that the transcriptional regulation activity of CBP for *CrebA* expression might also be affected through its sequestration by polyQ proteins. To test this hypothesis, we examined the localization of CBP in C4 da neurons overexpressing CBP (*CBP OE*) and found that CBP showed a diffuse localization pattern throughout the nucleus but a mixed pattern of diffused and punctate localization in the cytoplasm (Figure 7A). However, co-overexpression of CBP with 78Q in C4 da neurons (*78Q OE* + *CBP OE*) led to the co-localization of CBP with 78Q puncta in the nucleus and the disappearance of the original diffuse localization (Figure 7B). To further test the functional inhibition of CBP by polyQ proteins, we examined the capability of CBP to restore the polyQ-induced loss of GOPs when a stronger allele of 78Q (78Qs) was used. The restoration of GOPs by CBP overexpression was markedly diminished with the expression of 78Qs (Figure 7C), compared to the expression of a weak 78Q allele (Figure 6A). These data together suggest a possible sequestration of CBP by 78Q in C4 da neurons, which contributes to the inhibition of CBP-mediated GOP synthesis by 78Q. Unlike CBP, Cut showed no mis-localization in da neurons expressing 78Q (Figure S7B), suggesting that Cut may not be a strong interactor of polyQ proteins, consistent with the observation that Cut overexpression failed to restore the loss of GOPs under polyQ-expressed condition (Figure S7A).

DISCUSSION

Toxic nuclear polyQ proteins cause terminal dendrite defects in C4 da neurons. In this study, we propose a mechanistic model that links toxic nuclear polyQ proteins to the impaired elongation of terminal dendrites in *78Q OE* through the CBP-CrebA-COPII-GOP pathway (Figure 7D). Toxic nuclear polyQ proteins decreased the number of GOPs in the dendrites of C4 da neurons (Figure 2). mRNA sequencing revealed that the secretory pathway, including the COPII pathway, was a major pathway that was downregulated by toxic polyQ proteins (Figure 3). The disruption of the COPII pathway decreased GOP synthesis (Figure S4). TF enrichment analysis identified CrebA as a key regulator of the genes involved in the COPII pathway (Figure 4). CrebA overexpression restored the downregulation of the COPII pathway and the loss of GOPs caused by toxic polyQ proteins (Figure 4). We further found that CBP regulated *CrebA* expression cooperatively with Cut (Figure 6) and that toxic polyQ proteins interfered with CBP upstream of CrebA in the regulation of GOP synthesis (Figure 7). Finally, the co-overexpression of CrebA and Rac1 synergistically restored polyQ-induced defects in dendrite branching and elongation (Figure 5).

According to our mechanistic model (Figure 7D), however, how the overexpression of Cut, unlike CBP, can potentially contribute to the restoration of GOPs is unclear, although it cooperatively regulates CrebA expression with CBP (Figure 6I) and interacts with CBP at the protein level (Figure 6F). This can be explained by alterations in the stoichiometry between CBP and Cut for their complex formation under polyQ-expressed conditions. Our results showed that polyQ proteins appeared to sequester CBP, but not Cut. The sequestration of CBP by polyQ proteins leads to a decreased amount of CBP available for the CBP-Cut complex formation. Accordingly, CBP overexpression can increase the amount of non-sequestered CBP under polyQ-expressed conditions, thereby restoring the CBP-Cut complex formation. By contrast, Cut overexpression does not contribute to an increase in complex formation because it has no effect on the depletion of CBP by polyQ proteins. Moreover, we included Rac1 as a component in our mechanistic model (Figure 7D). Rac1 was connected to the polyQ-CBP-CrebA pathway based on the following results. We first tested whether polyQ expression affected the expression of *Rac1* and found a significant decrease in *Rac1* expression in polyQ-expressing fly heads compared to *w1118* (Figure 3G). We then searched for TFs that could be affected by polyQ expression and could regulate *Rac1* expression. Previously, Cut was shown to regulate *Rac1* expression (Jinushi-Nakao et al., 2007). Thus, to examine the effect of polyQ proteins on Cut, we checked whether polyQ proteins altered the intracellular distribution of Cut proteins in polyQ-expressing da neurons and found no noticeable alteration in its distribution (Figure S7B). As previously mentioned, we showed that Cut interacted with CBP in fly heads (Figure 6F). Furthermore, *Rac1* was shown to be epigenetically suppressed by H3K27me3 (Golden et al., 2013), which can be antagonized by CBP-dependent H3K27ac. These data together provide a mechanistic connection of the CBP-Cut-Rac1 pathway to the polyQ-CBP-CrebA pathway through CBP, as shown in Figure 7D.

In this study, we proposed a polyQ-CBP-CrebA pathway for polyQ-induced terminal dendrite defects. However, an alternative possibility that dendrite perturbation may precede through CBP-CrebA-independent pathways, which then can result in altered gene expression, cannot be excluded. Consistent with such a possibility, nuclear polyQ proteins were shown to sequester nuclear pore complex proteins, potentially impairing the transport of proteins and RNA, independently of CBP or CrebA (Grima et al., 2017). Moreover, nuclear polyQ proteotoxicity induces the mis-localization of several TFs (e.g., TBP, Sp1, and p53) other than CBP (Orr and Zoghbi, 2007), leading to the altered expression of their target genes. The perturbed functions of nuclear pore complexes and TFs may result in dendrite defects via CBP-CrebA-independent mechanisms and consequently alterations in gene expression. However, the restoration of GOP synthesis and PM protein supply via the overexpression of CBP or CrebA and the restoration of dendritic arborization defects via the co-overexpression of CrebA and Rac1 in polyQ-expressing neurons demonstrates that the CBP-CrebA pathway should be one of the important pathways that functionally regulates the polyQ-induced dendrite defects

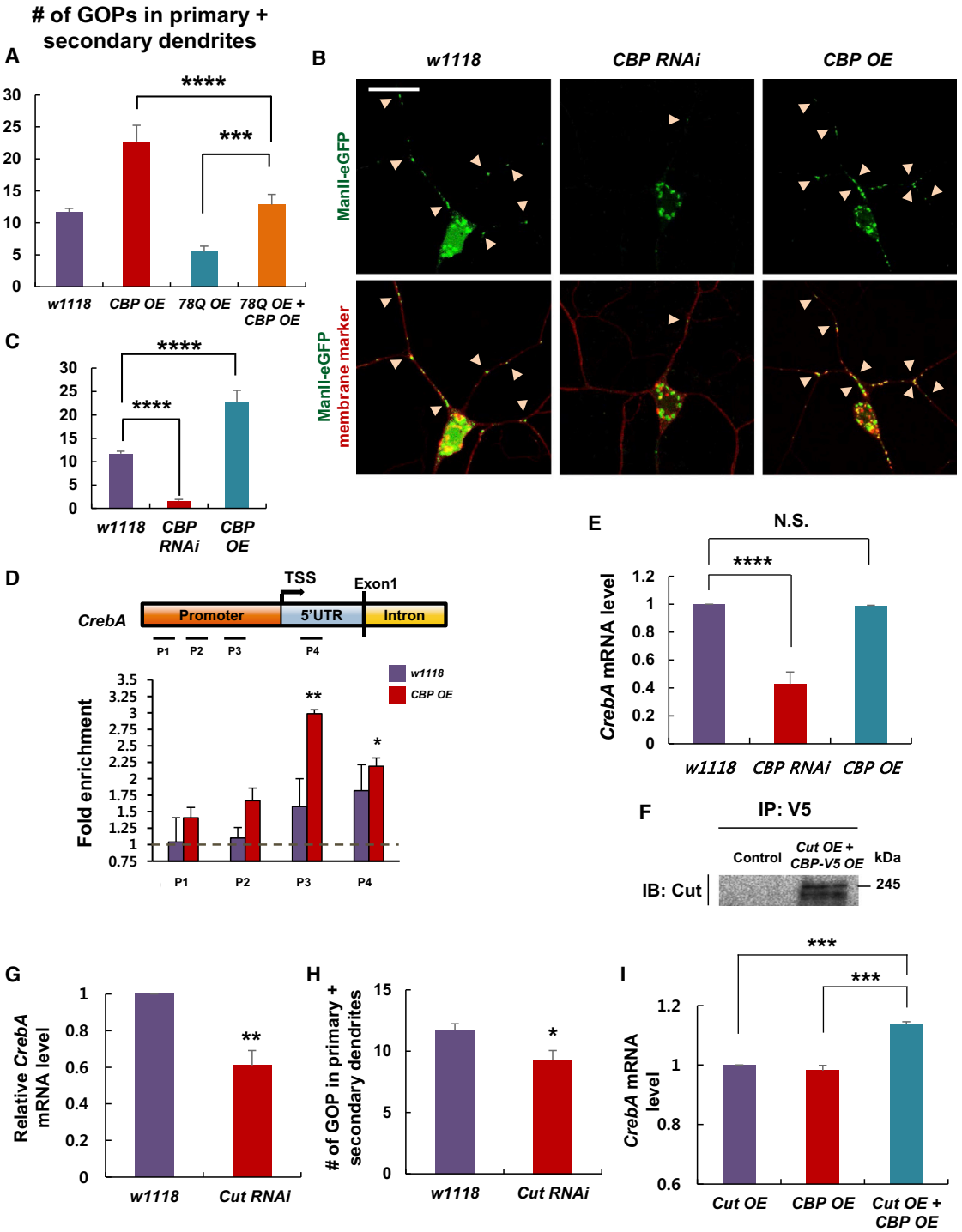

Figure 6. CBP Directly Regulates *CrebA* Transcription in Cooperation with Cut

(A) Quantification of the number of GOPs in the primary and secondary dendrites of *w1118* and C4 da neurons expressing the denoted transgenes. ***$p < 0.001$; ****$p < 0.10 \times 10^{-3}$ by two-way ANOVA with Tukey's post hoc correction; error bars, SEM; $n \geq 12$.

(B) Representative images of GOPs labeled by ManII-eGFP in *w1118*, *CBP RNAi*, and *CBP OE*. PM marker is in red (ppk-CD4-tdTom). GOPs are indicated by arrowheads. The scale bar represents 20 μm.

(C) Quantification of the number of GOPs in both primary and secondary dendrites of *w1118*, *CBP RNAi*, and *CBP OE*. ****$p < 0.10 \times 10^{-3}$ by one-way ANOVA with Tukey's post hoc correction; error bars, SEM; $n \geq 14$.

(legend continued on next page)

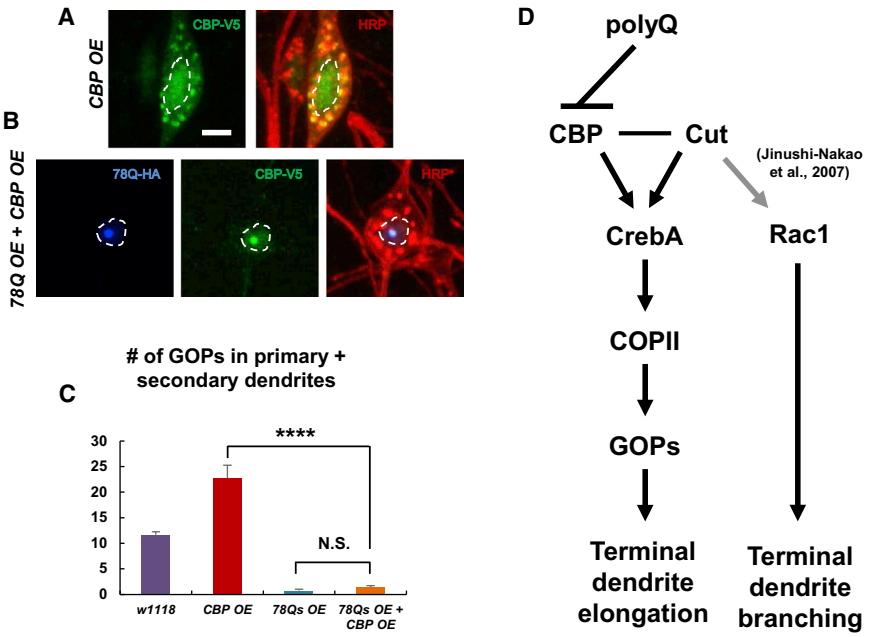

Figure 7. CBP Mis-localization Mediates the PolyQ-Induced Loss of GOPs

(A and B) Immunostaining of overexpressed CBP tagged with V5 in C4 da neurons with (B) or without (A) 78Q expression. CBP and 78Q were visualized with anti-V5 (green) and anti-HA antibodies (blue), respectively. PM was visualized with an anti-horseradish peroxidase (HRP) antibody (red). The nucleus is outlined by white dotted lines. The scale bar represents 5 μm.

(C) Quantification of the number of GOPs in the primary and secondary dendrites of *w1118* and C4 da neurons expressing the denoted transgenes. Note, the strong allele of 78Q (*78Qs*) was used here. ****$p < 0.10 \times 10^{-3}$ by two-way ANOVA with Tukey's post hoc correction; error bars, SEM; $n \geq 12$.

(D) Proposed mechanistic model for polyQ-induced terminal dendrite defects (branching and elongation). Black lines denote functional links identified by the experimental data in this study, whereas the gray line denotes the link identified by the indicated previous study.

(Figures 4B–4E, 5D, 5E, and 6A). Nevertheless, the relative importance of the CBP-CrebA pathway to the pathways that include other TFs affected by polyQ proteins can be questioned. However, we found that the overexpression of the three key TFs (*HLH106*, *gt*, and *Dref*) did not restore the number of GOPs in polyQ-expressing neurons (Figure S5A). Moreover, we also examined the effect of Sp1, which is known to be downregulated by polyQ proteins (Zhai et al., 2005), on GOP synthesis and found that *Sp1* knockdown did not significantly decrease the number of GOPs compared to the controls (Figure S7C). Furthermore, we also found that the overexpression of Cut and Scr, known upstream TFs of CrebA (Henderson and Andrew, 2000; Iyer et al., 2013), failed to restore the loss of GOPs in polyQ-expressing neurons comparable to CrebA overexpression (Figures 4B, 4C, and S7A). Therefore, our data suggest that the mechanism by which polyQ toxicity induces dendrite pathology can be attributed to the polyQ-CBP-CrebA pathway proposed in this study.

The loss of GOPs was one of the most apparent dendrite defects caused by polyQ proteins (Figures 2A and 2B). Thus, among many cellular processes downregulated by the polyQ proteins, we focused on three cellular processes (VT, MO, and LP) that we considered to be related to GOPs (Figure 3). However, these processes can also be related to other secretory-pathway-related processes in addition to GOP synthesis. For example, neuropeptide maturation and trafficking were previously shown to be modulated by the secretory pathway (Zhang et al., 2010), suggesting the potential association of neuropeptide-containing vesicle trafficking with the three processes. We thus examined the effect of polyQ proteins on neuropeptide-containing vesicle trafficking by measuring the amount of neuropeptide-containing vesicles in *w1118* and polyQ-expressing neurons using a reporter (ANF-EMD; Rao et al., 2001). We found that polyQ expression decreased the amount of ANF-EMD vesicles in dendrites and soma compared to controls (Figure S7D), suggesting that polyQ perturbs the function of the secretory pathway related to neuropeptide-containing vesicle trafficking in addition to GOP synthesis. Additionally, the three processes can be associated with the synthesis of somatic Golgi. However, our data showed a larger loss of ManII-eGFP-positive puncta in the dendrites of C4 da neurons compared to the soma (Figure 2C), suggesting that the three processes can be considered to be related more to GOP synthesis than to somatic Golgi synthesis. Thus, although the polyQ-induced downregulation of genes associated with the abovementioned three processes may impact the secretory pathway in general, our results appear to indicate that the synthesis of GOPs responds more to the

(D) ChIP-qPCR results showing that the promoter regions (P3 and P4) of *CrebA* exhibit increased CBP-V5 occupancy compared to the controls. *$p < 0.05$; **$p < 0.01$ by Student's t test; error bars, SEM; $n = 3$. Locations of four primers (P1–P4) used for qPCR experiments are denoted in the promoter and 5′ UTRs.

(E) *CrebA* mRNA expression level in fly brains of *w1118*, *CBP RNAi*, and *CBP OE*. ****$p < 0.10 \times 10^{-3}$ by one-way ANOVA with Tukey's post hoc correction; error bars, SEM; $n = 5$.

(F) Co-immunoprecipitation (coIP) of V5-tagged CBP proteins and Cut from the fly brains co-overexpressing Cut and CBP-V5 using *elav*-gal4.

(G) Relative mRNA expression level of *CrebA* in fly brains of *Cut RNAi* to that in *w1118*. **$p < 0.01$ by Student's t test; error bars, SEM; $n = 4$.

(H) Quantification of the number of GOPs in both primary and secondary dendrites of *w1118* and *Cut RNAi*. *$p < 0.05$ by Student's t test; error bars, SEM; $n \geq 20$.

(I) Relative mRNA expression levels of *CrebA* in fly brains of *CBP OE* and *Cut OE + CBP OE* to that in *Cut OE*. ***$p < 0.001$ by one-way ANOVA with Tukey's post hoc correction; error bars, SEM; $n = 3$.

See also Figure S7.

downregulation of those genes compared to the synthesis of somatic Golgi.

In mRNA-sequencing analysis, we used fly heads to identify genes affected by toxic polyQ proteins (Figure 3A). Considering that fly heads contain no C4 da neurons, alterations in gene expression obtained from mRNA sequencing in polyQ-expressing fly heads, compared to *w1118* fly heads, should be defined by non-C4 da cells. Due to a small number (~50) of C4 da neurons per larva, however, it is challenging to isolate a sufficient number ($\geq 10^5$ cells) of C4 da neurons for mRNA sequencing. Instead of C4 da neurons, we therefore used fly heads for mRNA sequencing to obtain a clue for alteration of gene expression by polyQ proteins. Moreover, mRNA sequencing identified 5,385 DEGs ($p < 0.05$) between polyQ-expressed and control samples (Table S1), of which 5,325 (98.9%) were downregulated. Such a large number and high percentage of downregulated genes suggests that there might be widespread cell death in polyQ-expressing fly brains. Thus, we checked the extent of cell loss in the polyQ-expressing adult fly brains on which mRNA sequencing was performed by measuring the number of cells that displayed cleaved caspase-3 through immunohistochemistry analysis. PolyQ-expressing brains showed minimal cell loss compared to controls in the condition where mRNA sequencing was performed (Figures S7E and S7F). Additionally, we found no observable decrease in rRNA in polyQ-expressed adult fly heads compared to *w1118* heads (Figure S7G). These data suggest that the downregulation of the large number of genes is not likely to be caused by cell death. One alternative explanation can be the previously reported dysregulation of the following histone modifications caused by polyQ proteins: impaired acetylation of H3K27 (Chou et al., 2014) and dysregulated tri-methylation of H3K9 (Ryu et al., 2006) and H3K27 (Seong et al., 2010). These dysregulated histone modifications may result in the downregulation of 98.9% of DEGs through a global epigenetic silencing.

The normal length of the polyQ tract in humans has been reported to be less than 36 for the MJD protein. In flies, numerous studies have used the truncated MJD protein with only 27 polyQ repeats (MJDtr-27Q) as a control (Saitoh et al., 2015; Warrick et al., 1998). However, in this study, we used *w1118* rather than *27Q OE* as the control for *78Q OE* in most of the experiments (Figures 1, 3, 4, 5, 6, and 7) because *27Q OE* exhibited strong dendrite pruning defects compared to *78Q OE* (Figures S7H and S7I). Previously, Kirilly et al. (2011) also showed that Httex1p-Q93 caused strong pruning defects in C4 da neurons, whereas Httex1p-Q20 caused no such defects. Taken together, these data suggest that the pruning defects are likely not due to the context of the host proteins but to polyQ toxicity. However, there appears to be a threshold length (between 20Q and 27Q) of the polyQ tract to confer such polyQ toxicity. Nevertheless, further detailed studies should be performed to understand the mechanism underlying the protein toxicity of MJDtr-27Q to induce pruning defects.

Finally, in this study, we identified three different nuclear polyQ toxicity models that exhibited decreased GOP synthesis (Figure S2B) and PM protein supply (Figure S2F), indicating a potentially shared mode of nuclear proteotoxicity. Of note, the accumulation of misfolded proteins in the nucleus has been observed in other neuronal diseases or during aging (De Cecco et al., 2011; Woulfe, 2007). Thus, our proposed mechanistic model underlying terminal dendrite defects caused by the accumulation of nuclear toxic polyQ proteins can provide significant insights into other neuronal maladies linked to nuclear proteotoxicity and aging that can be further examined in detailed functional studies.

EXPERIMENTAL PROCEDURES

Fly Stocks

The following lines were obtained from the Bloomington *Drosophila* Stock Center: *w1118*; *UAS-MJDtr-27Q* (*27Q*); *UAS-MJDtr-78Qs* (*78Qs*; II); *UAS-MJDtr-78Q* (*78Q*; III); *UAS-SNCA A30P*; *UAS-RedStinger*; *UAS-Rac1*; *UAS-CBP-V5*; *UAS-CBP RNAi*; *UAS-ANF-EMD*; *elav-gal4* (III); *elavGS-gal4* (III); *UAS-cut RNAi*; *UAS-Scr*; *UAS-CrebA*; *UAS-Sp1 RNAi*; *UAS-Sec23 RNAi*; and *UAS-Sec31 RNAi*. We did not use *27Q* as controls for most experiments due to an unforeseen toxicity, especially in the adult flies, when expressed pan-neuronally (data not shown). Most of the controls used in this study are *w1118* (gal4 only or with plasma membrane marker transgenes). The stocks and crosses were maintained in a 25°C incubator with 60% humidity. See Supplemental Information for other fly stocks.

Microscope Image Acquisition

Images of live third instar larvae using Leica SP5, Zeiss LSM700, or LSM780 confocal microscopes were processed with the Adobe Photoshop program, ImageJ, Neurolucida (MBF Bioscience), or Imaris (Bitplane). See Supplemental Information for more details.

Statistical Analysis

Two-tailed (except for when validating the downregulated gene expression pattern, in which case a one-tailed test was used) Student's t test assuming unequal variance (Microsoft Office Excel's TTEST) was used for statistical comparisons. When comparing three or more groups, one-way or two-way ANOVA was used and Tukey's post hoc correction was applied to adjust the p values accordingly. The SEM was used to generate error bars, unless otherwise specified. Note that comparisons of the number of GOPs, number of dendritic branches, and fluorescence intensity involving controls (*w1118*) were performed multiple times and pooled together into one dataset and were used throughout the entire manuscript with the exception of Figure 2. Likewise, the experimental groups *78Q OE*, *78Q OE + Rac1 OE*, and *CBP OE* were similarly analyzed.

ACCESSION NUMBERS

The accession number for the mRNA sequencing data reported in this paper is GEO: GSE65538.

SUPPLEMENTAL INFORMATION

Supplemental Information includes Supplemental Experimental Procedures, seven figures, and three tables and can be found with this article online at http://dx.doi.org/10.1016/j.celrep.2017.06.059.

AUTHOR CONTRIBUTIONS

C.G.C., M.J.K., K.H.J., D.H., and S.B.L. conceived the project, and C.G.C., M.J.K., K.H.J., M.H.H., J.H.P., I.J.C., G.R.K., J.H.C., Kunhyung Kim, and Keetae Kim performed experiments. D.Y.H., S.R., and H.J. performed mRNA sequencing and analyzed the data, and J.W.L. and K.P.K. performed lipidomics. C.G.C., M.J.K., K.H.J., M.D.E., T.K., D.H., and S.B.L. interpreted the data and wrote the manuscript.

ACKNOWLEDGMENTS

We would like to thank Dr. Joshua Bagley (IMBA, Vienna) for helpful discussion and critique on our manuscript. This work was supported by the DGIST R&D and MIREBraiN program, Basic Science Research Program through the Ministry of Science, ICT, and Future Planning of Korea (17-BD-0402, 17-BT-02, and 17-01-HRSS-02), the Development of Platform Technology for Innovative Medical Measurements Program from the Korea Research Institute of Standards and Science (KRISS-2017-GP2017-0020; to S.B.L.), and The Institute for Basic Science (IBS-R013-G1; to D.H.) funded by the Ministry of Science, ICT, and Future Planning of Korea.

Received: August 18, 2016
Revised: April 28, 2017
Accepted: June 21, 2017
Published: July 11, 2017

REFERENCES

Abrams, E.W., and Andrew, D.J. (2005). CrebA regulates secretory activity in the Drosophila salivary gland and epidermis. Development *132*, 2743–2758.

Anderson, J., Bhandari, R., and Kumar, J.P. (2005). A genetic screen identifies putative targets and binding partners of CREB-binding protein in the developing Drosophila eye. Genetics *171*, 1655–1672.

Bankaitis, V.A., Garcia-Mata, R., and Mousley, C.J. (2012). Golgi membrane dynamics and lipid metabolism. Curr. Biol. *22*, R414–R424.

Capovilla, M., Eldon, E.D., and Pirrotta, V. (1992). The giant gene of Drosophila encodes a b-ZIP DNA-binding protein that regulates the expression of other segmentation gap genes. Development *114*, 99–112.

Chae, S., Ahn, B.Y., Byun, K., Cho, Y.M., Yu, M.H., Lee, B., Hwang, D., and Park, K.S. (2013). A systems approach for decoding mitochondrial retrograde signaling pathways. Sci. Signal. *6*, rs4.

Chou, A.H., Chen, Y.L., Hu, S.H., Chang, Y.M., and Wang, H.L. (2014). Polyglutamine-expanded ataxin-3 impairs long-term depression in Purkinje neurons of SCA3 transgenic mouse by inhibiting HAT and impairing histone acetylation. Brain Res. *1583*, 220–229.

De Cecco, M., Jeyapalan, J., Zhao, X., Tamamori-Adachi, M., and Sedivy, J.M. (2011). Nuclear protein accumulation in cellular senescence and organismal aging revealed with a novel single-cell resolution fluorescence microscopy assay. Aging (Albany NY) *3*, 955–967.

Eberlé, D., Hegarty, B., Bossard, P., Ferré, P., and Foufelle, F. (2004). SREBP transcription factors: master regulators of lipid homeostasis. Biochimie *86*, 839–848.

Fox, R.M., Hanlon, C.D., and Andrew, D.J. (2010). The CrebA/Creb3-like transcription factors are major and direct regulators of secretory capacity. J. Cell Biol. *191*, 479–492.

Golden, S.A., Christoffel, D.J., Heshmati, M., Hodes, G.E., Magida, J., Davis, K., Cahill, M.E., Dias, C., Ribeiro, E., Ables, J.L., et al. (2013). Epigenetic regulation of RAC1 induces synaptic remodeling in stress disorders and depression. Nat. Med. *19*, 337–344.

Grima, J.C., Daigle, J.G., Arbez, N., Cunningham, K.C., Zhang, K., Ochaba, J., Geater, C., Morozko, E., Stocksdale, J., Glatzer, J.C., et al. (2017). Mutant Huntingtin disrupts the nuclear pore complex. Neuron *94*, 93–107.e6.

Han, C., Jan, L.Y., and Jan, Y.N. (2011). Enhancer-driven membrane markers for analysis of nonautonomous mechanisms reveal neuron-glia interactions in Drosophila. Proc. Natl. Acad. Sci. USA *108*, 9673–9678.

Hanus, C., and Ehlers, M.D. (2008). Secretory outposts for the local processing of membrane cargo in neuronal dendrites. Traffic *9*, 1437–1445.

Hasel, P., McKay, S., Qiu, J., and Hardingham, G.E. (2015). Selective dendritic susceptibility to bioenergetic, excitotoxic and redox perturbations in cortical neurons. Biochim. Biophys. Acta *1853*, 2066–2076.

Henderson, K.D., and Andrew, D.J. (2000). Regulation and function of Scr, exd, and hth in the Drosophila salivary gland. Dev. Biol. *217*, 362–374.

Hong, J.H., Kang, J.W., Kim, D.K., Baik, S.H., Kim, K.H., Shanta, S.R., Jung, J.H., Mook-Jung, I., and Kim, K.P. (2016). Global changes of phospholipids identified by MALDI imaging mass spectrometry in a mouse model of Alzheimer's disease. J. Lipid Res. *57*, 36–45.

Horton, A.C., Rácz, B., Monson, E.E., Lin, A.L., Weinberg, R.J., and Ehlers, M.D. (2005). Polarized secretory trafficking directs cargo for asymmetric dendrite growth and morphogenesis. Neuron *48*, 757–771.

Huang da, W., Sherman, B.T., and Lempicki, R.A. (2009). Systematic and integrative analysis of large gene lists using DAVID bioinformatics resources. Nat. Protoc. *4*, 44–57.

Hughes, R.E. (2002). Polyglutamine disease: acetyltransferases awry. Curr. Biol. *12*, R141–R143.

Hughes, C.L., and Thomas, J.B. (2007). A sensory feedback circuit coordinates muscle activity in Drosophila. Mol. Cell. Neurosci. *35*, 383–396.

Iyer, S.C., Ramachandran Iyer, E.P., Meduri, R., Rubaharan, M., Kuntimaddi, A., Karamsetty, M., and Cox, D.N. (2013). Cut, via CrebA, transcriptionally regulates the COPII secretory pathway to direct dendrite development in Drosophila. J. Cell Sci. *126*, 4732–4745.

Jan, Y.N., and Jan, L.Y. (2010). Branching out: mechanisms of dendritic arborization. Nat. Rev. Neurosci. *11*, 316–328.

Jinushi-Nakao, S., Arvind, R., Amikura, R., Kinameri, E., Liu, A.W., and Moore, A.W. (2007). Knot/Collier and cut control different aspects of dendrite cytoskeleton and synergize to define final arbor shape. Neuron *56*, 963–978.

Kirilly, D., Wong, J.J., Lim, E.K., Wang, Y., Zhang, H., Wang, C., Liao, Q., Wang, H., Liou, Y.C., Wang, H., and Yu, F. (2011). Intrinsic epigenetic factors cooperate with the steroid hormone ecdysone to govern dendrite pruning in Drosophila. Neuron *72*, 86–100.

Koval, M., and Pagano, R.E. (1991). Intracellular transport and metabolism of sphingomyelin. Biochim. Biophys. Acta *1082*, 113–125.

Kweon, J.H., Kim, S., and Lee, S.B. (2017). The cellular basis of dendrite pathology in neurodegenerative diseases. BMB Rep. *50*, 5–11.

Lee, S.B., Bagley, J.A., Lee, H.Y., Jan, L.Y., and Jan, Y.N. (2011). Pathogenic polyglutamine proteins cause dendrite defects associated with specific actin cytoskeletal alterations in Drosophila. Proc. Natl. Acad. Sci. USA *108*, 16795–16800.

Li, S., Aufiero, B., Schiltz, R.L., and Walsh, M.J. (2000). Regulation of the homeodomain CCAAT displacement/cut protein function by histone acetyltransferases p300/CREB-binding protein (CBP)-associated factor and CBP. Proc. Natl. Acad. Sci. USA *97*, 7166–7171.

Matsukage, A., Hirose, F., Yoo, M.A., and Yamaguchi, M. (2008). The DRE/DREF transcriptional regulatory system: a master key for cell proliferation. Biochim. Biophys. Acta *1779*, 81–89.

Mikhaylova, M., Bera, S., Kobler, O., Frischknecht, R., and Kreutz, M.R. (2016). A Dendritic Golgi Satellite between ERGIC and Retromer. Cell Rep *14*, 189–199.

Murthy, M., Ranjan, R., Denef, N., Higashi, M.E., Schupbach, T., and Schwarz, T.L. (2005). Sec6 mutations and the Drosophila exocyst complex. J. Cell Sci. *118*, 1139–1150.

Orr, H.T., and Zoghbi, H.Y. (2007). Trinucleotide repeat disorders. Annu. Rev. Neurosci. *30*, 575–621.

Paccaud, J.P., Reith, W., Carpentier, J.L., Ravazzola, M., Amherdt, M., Schekman, R., and Orci, L. (1996). Cloning and functional characterization of mammalian homologues of the COPII component Sec23. Mol. Biol. Cell *7*, 1535–1546.

Papoulas, O., Hays, T.S., and Sisson, J.C. (2005). The golgin Lava lamp mediates dynein-based Golgi movements during Drosophila cellularization. Nat. Cell Biol. *7*, 612–618.

Pfenninger, K.H. (2009). Plasma membrane expansion: a neuron's Herculean task. Nat. Rev. Neurosci. *10*, 251–261.

Rao, S., Lang, C., Levitan, E.S., and Deitcher, D.L. (2001). Visualization of neuropeptide expression, transport, and exocytosis in Drosophila melanogaster. J. Neurobiol. *49*, 159–172.

Ryu, H., Lee, J., Hagerty, S.W., Soh, B.Y., McAlpin, S.E., Cormier, K.A., Smith, K.M., and Ferrante, R.J. (2006). ESET/SETDB1 gene expression and histone H3 (K9) trimethylation in Huntington's disease. Proc. Natl. Acad. Sci. USA *103*, 19176–19181.

Saitoh, Y., Fujikake, N., Okamoto, Y., Popiel, H.A., Hatanaka, Y., Ueyama, M., Suzuki, M., Gaumer, S., Murata, M., Wada, K., and Nagai, Y. (2015). p62 plays a protective role in the autophagic degradation of polyglutamine protein oligomers in polyglutamine disease model flies. J. Biol. Chem. *290*, 1442–1453.

Salama, N.R., Chuang, J.S., and Schekman, R.W. (1997). Sec31 encodes an essential component of the COPII coat required for transport vesicle budding from the endoplasmic reticulum. Mol. Biol. Cell *8*, 205–217.

Seong, I.S., Woda, J.M., Song, J.J., Lloret, A., Abeyrathne, P.D., Woo, C.J., Gregory, G., Lee, J.M., Wheeler, V.C., Walz, T., et al. (2010). Huntingtin facilitates polycomb repressive complex 2. Hum. Mol. Genet. *19*, 573–583.

Song, W., Onishi, M., Jan, L.Y., and Jan, Y.N. (2007). Peripheral multidendritic sensory neurons are necessary for rhythmic locomotion behavior in Drosophila larvae. Proc. Natl. Acad. Sci. USA *104*, 5199–5204.

Theopold, U., Ekengren, S., and Hultmark, D. (1996). HLH106, a Drosophila transcription factor with similarity to the vertebrate sterol responsive element binding protein. Proc. Natl. Acad. Sci. USA *93*, 1195–1199.

van Meer, G., Voelker, D.R., and Feigenson, G.W. (2008). Membrane lipids: where they are and how they behave. Nat. Rev. Mol. Cell Biol. *9*, 112–124.

Warrick, J.M., Paulson, H.L., Gray-Board, G.L., Bui, Q.T., Fischbeck, K.H., Pittman, R.N., and Bonini, N.M. (1998). Expanded polyglutamine protein forms nuclear inclusions and causes neural degeneration in Drosophila. Cell *93*, 939–949.

Woulfe, J.M. (2007). Abnormalities of the nucleus and nuclear inclusions in neurodegenerative disease: a work in progress. Neuropathol. Appl. Neurobiol. *33*, 2–42.

Ye, B., Zhang, Y., Song, W., Younger, S.H., Jan, L.Y., and Jan, Y.N. (2007). Growing dendrites and axons differ in their reliance on the secretory pathway. Cell *130*, 717–729.

Zhai, W., Jeong, H., Cui, L., Krainc, D., and Tjian, R. (2005). In vitro analysis of huntingtin-mediated transcriptional repression reveals multiple transcription factor targets. Cell *123*, 1241–1253.

Zhang, X., Bao, L., and Ma, G.Q. (2010). Sorting of neuropeptides and neuropeptide receptors into secretory pathways. Prog. Neurobiol. *90*, 276–283.

Zhou, W., Chang, J., Wang, X., Savelieff, M.G., Zhao, Y., Ke, S., and Ye, B. (2014). GM130 is required for compartmental organization of dendritic golgi outposts. Curr. Biol. *24*, 1227–1233.